In: IET Radar 2022: International Conference on Radar Systems, Edinburgh, 24-27 October 2022.
DOI:10.1049/icp.2023.1255; https://ieeexplore.ieee.org/document/10106299

Non-overlapping trajectory Multistatic SAR Coherent Change Detection

Alexander Hagelberg[1*], Daniel Andre[1], Mark Finnis[2]

[1] Centre for Electronic Warfare, Information and Cyber, Cranfield University, Defence Academy of the United Kingdom, Shrivenham, UK.
[2] Centre for Defence Engineering, Cranfield University, Defence Academy of the United Kingdom, Shrivenham, UK.
**Alexander.Hagelberg@cranfield.ac.uk*

Keywords: SYNTHETIC APERTURE RADAR (SAR), K-SPACE, FOURIER DOMAIN, COHERENT CHANGE DETECTION (CCD), MULTISTATIC

Abstract

Synthetic Aperture Radar (SAR) Coherent Change Detection (CCD) allows the detection of very small scene changes but is typically reliant on a high degree of similarity in the radar trajectories, with a small baseline. In the case of multistatic SAR imagery, such as those formed by a constellation of SAR satellites, the radar trajectories may have a greater baseline than those collected by a monostatic system such as an aircraft. This paper investigates the effects of multistatic trajectories on the measured coherence between imagery, and how this relates to the spatial frequency (K-space). In particular, the case where radar platform trajectories are greatly dissimilar, but where the K-space image supports still contains a high degree of overlap, is investigated. This paper uses multistatic SAR collections measured at the Ground Based SAR Laboratory at Cranfield University.

1. Introduction

Synthetic Aperture Radar (SAR) allows the formation of high-resolution radar images, and Coherent Change Detection (CCD) between two SAR images can highlight subtle changes between them [1]. Whilst CCD offers the potential for detecting small changes in the scene, it is reliant on a high degree of coherence between the two images. If there is a large degree of incoherence, then changes will be obscured and difficult to detect.

The choice of SAR imaging geometry will affect the corresponding complex Radar Cross Section (RCS) values over the imaged scene and will thus have an effect on the coherence between different bistatic SAR images [2, 3]. The coherence of scene areas dominated by speckle is due to scatterers within a resolution cell interfering, contributing to the amplitude and phase in the imagery. As the radar platform path changes so do these values [4]. If information from SAR radar platforms travelling different tracks could be used to accurately detect changes, this could allow for more rapid return scans of target locations. This work investigates the use of disparate bistatic radar trajectories for the collection of coherent SAR data, and is validated with measured data collected with the Ground Based SAR (GBSAR) system at Cranfield University [3, 5, 6] as well as simulations.

Multistatic and bistatic CCD geometries are becoming an increasingly viable proposition for remote sensing. The cost of launching payloads to orbit has reduced to below $2000 per Kg [7] depending on the launch vehicle. This makes the possibility of large SAR satellite constellations [8], or a powerful SAR satellite and ground-based aircraft receivers, a more feasible possibility. The current improved density and lower cost of high-performance computer components make processing large volumes of data possible in a reasonable timeframe. [3]

This paper begins with introducing some background concepts. The paper then discusses the methodology used (both experimental and simulation). There is then a results and discussion section followed by a conclusion.

2. Background

2.1. Coherent Change Detection

The coherence between two SAR images is calculate using the standard equation for CCD [3], giving the normalized complex cross correlation, whose magnitude γ is referred to as the sample (estimated) coherence.

$$\gamma e^{i\phi} = \frac{\sum_{k=1}^{N} S_1(k) S_2^*(k)}{\sqrt{\sum_{k=1}^{N} |S_1(k)|^2 \sum_{k=1}^{N} |S_2(k)|^2}} \quad (1)$$

Where S_1 and S_2 are the two complex images being compared and N is the number of pixels within a sample window which slides over the two images. The magnitude and phase of the complex correlation are γ and ϕ. The coherence is presented on a pixel-by-pixel basis to produce a coherence "CCD" image with values lying between 0 and 1, where 0 indicates no coherence, and 1 represents full coherence. An average can be taken over the CCD image representing overall coherence. The value of the estimated coherence varies with the choice of window size [4].

Published by IET. This is the Author Accepted Manuscript issued with: Creative Commons Attribution Non-Commercial License (CC:BY:NC 4.0).
The final published version (version of record) is available online at DOI:10.1049/icp.2023.1255. Please refer to any applicable publisher terms of use.

2.2. *Spatial frequency (K-space)*

The image support represented in the spatial frequency domain is typically in the form of an annulus segment. The spatial frequency can be conceptualised in two ways. The first is as a Fourier transform of an image, and the other as a composite of all incident and scattered wave vectors ($\boldsymbol{k}_i$ and $\boldsymbol{k}_s$) associated with the data collection, and here with a length proportional to frequency, for convenience.

$$\boldsymbol{k}_i = \hat{\boldsymbol{\imath}} \frac{2\pi f}{c} \tag{2}$$

$$\boldsymbol{k}_s = \hat{\boldsymbol{s}} \frac{2\pi f}{c} \tag{3}$$

$$\boldsymbol{K} = \boldsymbol{k}_i - \boldsymbol{k}_s \tag{4}$$

Here $\hat{\boldsymbol{\imath}}$ and $\hat{\boldsymbol{s}}$ represent the unit vectors of the incident and scattered wave directions respectively. $\boldsymbol{K}$ is the total wavenumber vector, which will be plotted in spatial frequency figures with units of GHz (multiplying $\boldsymbol{K}$ wavenumber value by c/4π). Each position in K-space corresponds to a single scattering measurement at a given frequency and for a given combination of receiver and transmitter positions.

When a whole SAR collection is presented in this way, this leads to characteristic image support shapes for SAR far-field measurements. However, when in the SAR near-field regime, wavefronts are significantly curved across the scene so that separate areas of the image have significantly different Fourier domain image supports, which we refer to as sub-supports. Here, the SAR near-field regime is defined to occur at ranges $d < 2L_{cr}^2 \lambda_c^{-1}$ for an image cross range extent L_{cr} and a centre wavelength λ_c .

Figure 1 shows five constituent sub-supports from a monostatic collection taken in the SAR near field projected onto the ground plane. These supports exhibit significant variation. Thus, for SAR near-field collections, processes such as trimming of incoherent energy [6, 10] will need to be spatially variant over the scene.

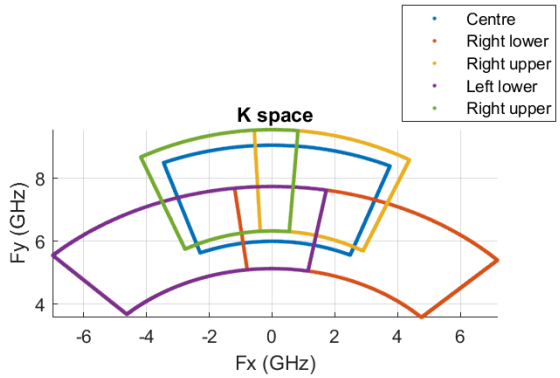

Figure 1. A plan view of the K-space sub-support outlines for the four corners of the gravel area and the centre (blue). This shows the variation in ground-plane resolution.

A key point to be noted for the current work, is that whilst two SAR platform trajectories may have little overlap in the spatial domain, the image supports may have a high degree of overlap in the spatial frequency domain, which could lead to high coherence between collections. This is a hypothesis which will be tested here.

2.3. *Coherence estimation*

The coherence in an image can be thought of as the product of three main effects. [4, 11]. These equations and papers were originally developed for monostatic geometries, we hypothesise that they remain valid for bistatic and multistatic scenarios.

$$\gamma = \gamma_{temp}\gamma_{snr}\gamma_{proc} \tag{5}$$

Here γ is *true coherence*, which differs from the *estimated* coherence in equation (*1*). The temporal correlation, γ_{temp}, is from changes in the scene. If there were no change in the scene, including environmental effects such as rain or wind, this would take a value tending to 1. If there were significant change in the scene, then the value would be close to 0. The other correlations contributing to the sample coherence are due to noise, γ_{snr}, and due to processing and spatial effects, γ_{proc} [4]

$$\gamma_{proc} = \gamma_{algorithm}\gamma_{baseline}\gamma_{RCS}\gamma_{registration} \tag{6}$$

Where, $\gamma_{algorithm}$ refers to errors arising from the SAR imaging algorithm approximations; the baseline effects, $\gamma_{baseline}$ arise from the mismatch in radar platform trajectories and in the resulting different imaging angles; and γ_{RCS} is the change in scatterer RCS as a function of SAR geometry and polarisation [2, 3]. The baseline factor $\gamma_{baseline}$ is related to the degree of overlap of the projected K-space image sub-supports. $\gamma_{baseline}$ can be increased (brought closer to 1) through the process of removing radar data which is not part of the two image support overlap areas in K-space, when these are projected onto the ground surface plane. This is a process known as incoherent energy trimming [2, 4, 10].

There is then a contribution due to the registration, $\gamma_{registration}$ [4]. These are typically seen as arising from the layover effect or an inaccurate ground truth/radar trajectory.

3. Methodology

3.1. *GBSAR laboratory*

The GBSAR laboratory performs microwave measurements with a Vector Network Analyser (VNA), which generates a stepped frequency waveform. The system is currently set up for indoor use, with the VNA attached to two Ultra-Wideband horn antennas allowing measurements within the range 1-10 GHz. The Antennae can be mounted in a bistatic or a pseudo monostatic configuration. When in a bistatic configuration, each antenna is mounted on a different two-dimensional vertical SAR aperture scanner. One SAR aperture is 3.5 m wide by 1.5 m high and is used for the transmitter. The other aperture is 1.285 m wide by 1.5 m high and is used for the receiver. These are shown in Figure 2. The measured target scene consisted of gravel (Figure 2), which provides a

developed speckle SAR image suitable for the coherence investigation. [3, 6]

3.2. *Laboratory measurement*

The data collection involved transmitter and receiver antenna mounted onto rails with two axis movement. The scene consisted of a rectangular gravel area with metal spheres positioned around it for alignment and validation of the images. When the scene is left untouched, and the scans are repeated with the receiver in a new location, the collection of scans are equivalent to a single multistatic scan with multiple receivers operating simultaneously. The full collection consisted of the transmitter scan at two heights for each of nine receiver positions (see Figure 4). For change detection '*GBSAR*' was traced lightly with a stick in the gravel.

Figure 2. The GBSAR laboratory in a bistatic configuration, measuring a gravel scene. The locations of the transmitter (Tx) and receiver (Rx) are marked. Several metal spheres are positioned around the gravel to aid alignment checks.

3.3. *Simulations*

This paper employs simulated data and measured experimental data for validation. The simulation employs the laboratory ground truth and measured SAR geometries.

The simulation assumes perfect isotropic point scatterers and does not account for shadowing or multipath [3]. It was ensured that fully developed speckle was present and that the intensity distribution across the Region of Interest (ROI) conformed to the Rayleigh distribution [3, 10]. A disturbance in the form of 'GBSAR' was used in simulated images.

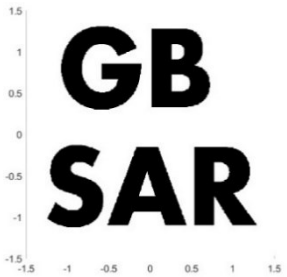

Figure 3. Plot showing the disturbance used in the simulated results.

3.4. *Radar trajectories*

When considering the trajectories to be used for CCD analysis it is typical to aim for these to be as similar as possible to improve the coherence. This paper uses collections and trajectories which have a significant difference in the spatial domain but maintain a significant K-space overlap [3].

The transmitter trajectories were chosen to have no positions in common, covering different sectors in Azimuth, whereas the grid of 9 fixed receiver positions remained the same (see Figure 4). The transmitter track was split into two halves, Tx1 and Tx2. The receivers were labelled 1-9 and are here referred to as Rx1-9.

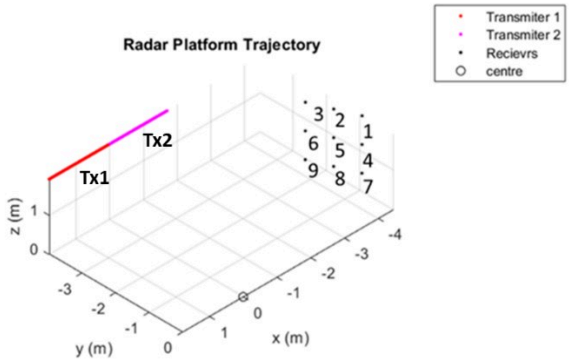

Figure 4. The radar trajectories in the data collection, shown split into two half apertures Tx1 and Tx2. The scene centre is also shown at (0,0).

There were 9 bistatic SAR geometries associated with each transmitter half aperture, hence there was 81 possible combinations for measuring SAR coherence. The 81 $\gamma_{baseline}$ coherence values were calculated for the 81 pairs and presented in Figure 5. It can be seen that the majority of trajectories exhibit zero overlap, thus only a few bistatic geometry were used in this study.

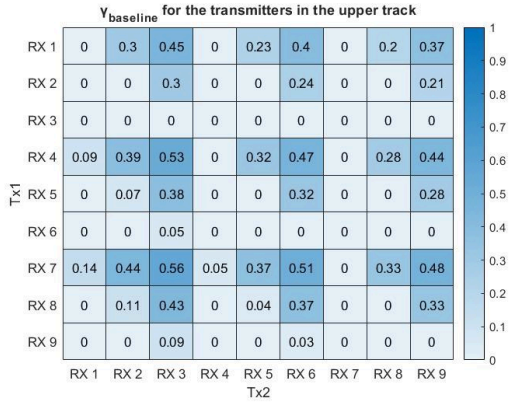

Figure 5. Heatmap showing calculated $\gamma_{baseline}$ for different bistatic geometry pairs.

3.5. *Data processing & incoherence trimming*

The SAR data, whether simulated or real is processed in the same manner and used the same frequency range of 6.6-10GHz. Consider a particular set of bistatic reference and mission trajectories. For these trajectories, the K-space

frequency sub-supports would vary across the scene, and an encompassing region of K-space is designated for analysis. Whether a K-space area in this region is occupied or not by a given sub-support, is calculated. The overlapping (coherent) and non-overlapping (incoherent) K-space sub-supports for the reference and mission collections are then found for each SAR image spatial position / imaging pixel. The non-overlapping areas can then be excluded from newly formed incoherence trimmed SAR images. This leaves trimmed reference and mission image pair [6, 12].

This process was implemented for all the bistatic SAR geometry pairs within the chosen multistatic collection. A trimmed multistatic reference image could then be formed as the coherent sum of all trimmed reference images, and a mission image in the same manner.

CCD algorithms were run, both on the full multistatic images and on the individual bistatic SAR image pairs.

4. Results

4.1. Low resolution simulations

A problem could be seen with some of the results where the K-space support overlap was low. In this case a large number of pulses were removed, giving the SAR image results with very poor cross-range resolution. This leaves large smears along ellipses of equal range, across the SAR images, instead of well-defined points. This effect was also seen in the spatially variant trimmed CCD images. Where large smears of incoherence are present, shown in Figure 6.

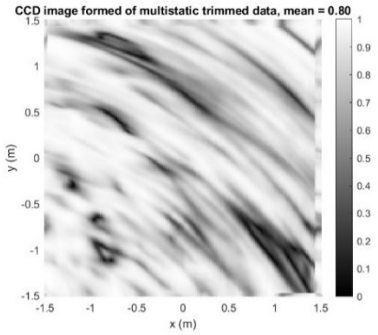

Figure 6. Simulated CCD image formed between Tx1-Rx8 and Tx2-Rx2. This clearly shows 'smears' of incoherence across the image.

These smears had the effect of adding large incoherence signatures to the multistatic images. The multistatic CCD images, such as in Figure 7, exhibited a speckly appearance and low coherence when including trajectories with a low overlap. These multistatic trimmed images were formed as coherent sums of the bistatic geometry SAR images, as explained in section 3.5. After all incoherent energy had been removed, the measured coherence was only around 0.64, substantially lower than the 0.8-0.9 expected if there were no scene disturbance. The disturbance 'GBSAR' (Figure 3) is not possible to identify in the CCD result.

This did demonstrate that simply adding bistatic geometries does not necessarily lead to improved CCD products. A careful choice of trajectories with an improved overlap would likely result in a significantly improved CCD image. This is shown in the next section.

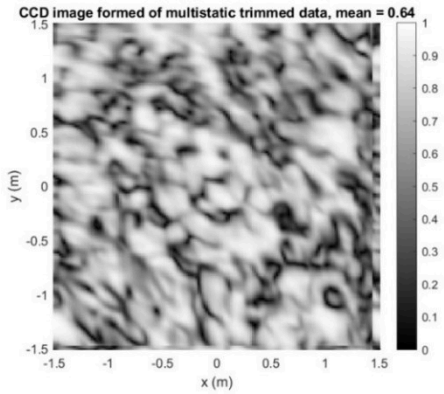

Figure 7. Simulated multistatic CCD image, showing a speckly result with the disturbance (Figure 3) indistinguishable. Formed using Tx1-Rx7&8 as the reference geometries and Tx2-Rx2&3 as the mission geometries.

4.2. High resolution simulation

Higher resolution simulations were next carried out, with Tx1 and Rx 7 against Tx2 and Rx 2&3. Tx1-Rx8 was omitted as it resulted in smearing, and as seen in Figure 5, has a very low overlap in the K-space. The trajectories are shown in Figure 8. In this case the multistatic CCD image had a high coherence of 0.91. The issue with cross range resolution remained to a degree, with some small smearing. This resulted in the disturbance being obscured somewhat.

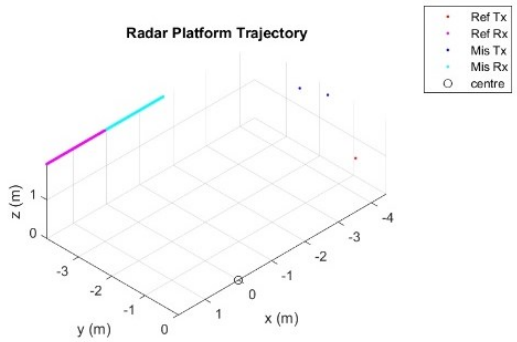

Figure 8. Radar trajectory used in forming the high resolution simulate multistatic images. Tx1-Rx7 was the reference geometry and Tx2-Rx2&3 were the mission geometries.

The resulting multistatic trimmed CCD image, seen in Figure 9, was of good quality, however some letters were difficult to make out. This is particularly evident on the S and A. The disturbance is however clearly distinct from the undisturbed gravel background.

Additional CCD results could be produced in addition to the multistatic CCD image. Multiple CCD images were produced for the bistatic SAR geometries within the multistatic collection. Each pixel within the CCD image would now have multiple complex correlation values associated with it from the

multiple bistatic CCD images produced. Forming a new image using the average per pixel value resulted in Figure 10 (a). This CCD image had a lower coherence than the multistatic CCD (0.77 compared to 0.83), however the letters were more legible. Taking the maximum per pixel value resulted in Figure 10 (b). This CCD image exhibited a higher coherence than the multistatic CCD image (0.88 compared to 0.83). whilst the disturbance is clear, the shapes of some of the letters remain hard to identify.

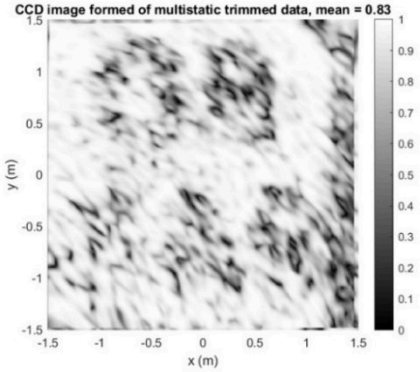

Figure 9. CCD image of simulated multistatic fully trimmed SAR images. The disturbance is visible, but it is difficult to identify the shapes.

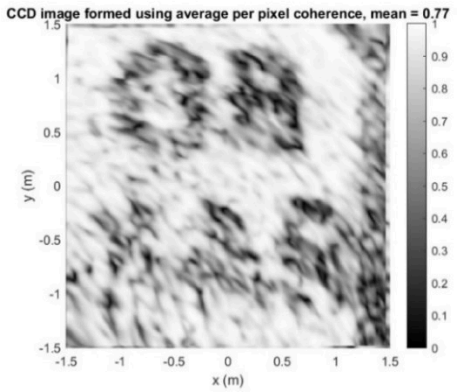

(a)

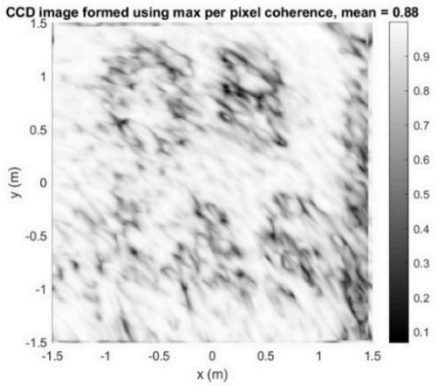

(b)

Figure 10. CCD products formed using the averaged (a) or maximum (b) per pixel values from fully trimmed bistatic images.

It is possible that using multiple passes leads to an improvement as each image had a different cross range direction. This may have resulted in the effect of the elongated speckle components being reduced. Resolution will not have been improved as the bandwidth and azimuth angles remained the same. It is possible that multipass algorithms may be beneficial in detecting small changes when compared to using multistatic images.

4.3. Measured results

Attempting CCD analysis of the measured data proved more difficult as the gravel stones were not isotropic scatterers. As such, despite trimming off incoherent energy there was still a substantial decorrelation. This is likely caused by the change in the path of the backscatter and thus a phase change. In the best-case scenario, where the reference and mission trajectories were the same, the CCD image was of high quality. This is shown in Figure 11. The VV polarisation was used for the measured results in this paper.

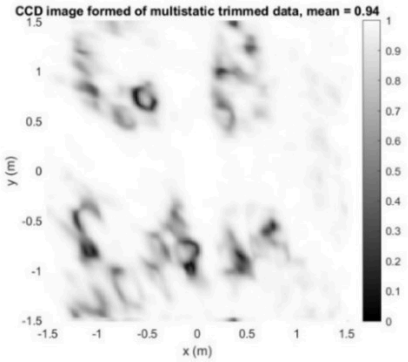

Figure 11. CCD image for measured data. Tx1Rx7 and VV polarisation. The 'GBSAR' disturbance is quite clear against the background.

When a resolution cell contains multiple scatterers, each contributing an unstable amplitude and phase, any change in radar geometry can be expected to lead to decorrelation [4] as the path taken by backscatter changes. When combined with the changing RCS of the gravel with respect to azimuth angle, the measured CCD results were of poorer quality. The multistatic CCD image shown in Figure 12 is significantly less clear than the simulated results or exact repeating trajectory shown in Figure 11. This is also true for the results in Figure 13 show that using average or maximum per pixel values of CCD's formed using bistatic geometries did not provide any improvement in legibility.

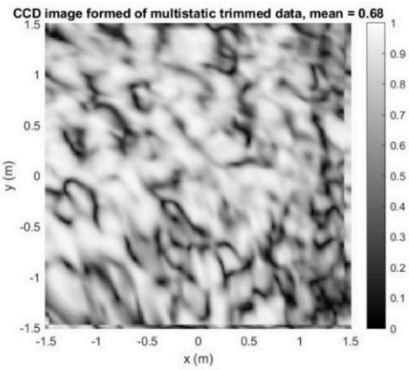

Figure 12. Multistatic measured (real) CCD image. This image shows a higher degree of decorrelation and results in the 'GBSAR' being obscured and not legible.

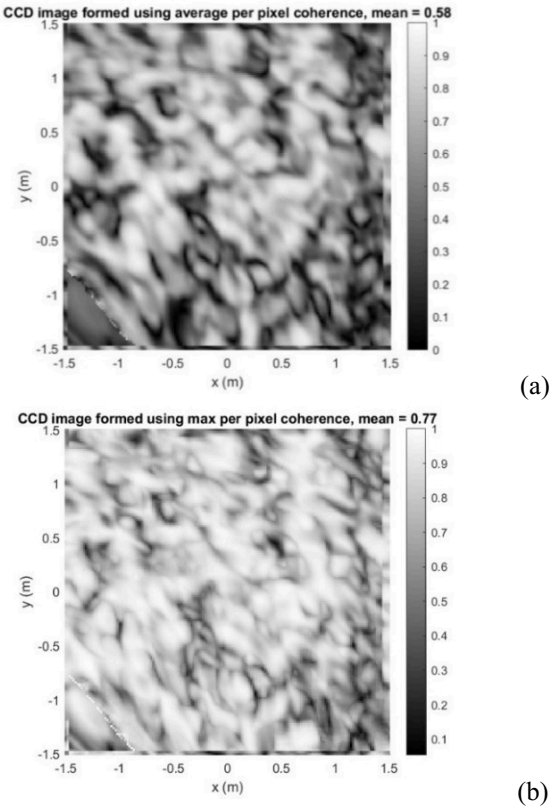

Figure 13. CCD products formed using the averaged (a) or maximum (b) per pixel values from fully trimmed measured bistatic images.

5. Discussion & Conclusion

The simulated results were promising, showing the disturbance clearly, the real results however were much less clear. This can partly be attributed to the disturbance, as the measured data had a smaller and less severe disturbance which made it much more difficult to identify when the surrounding gravel had a low coherence. The non-isotropic nature of the gravel will also have contributed to the quality of the results. It is recognised that these factors make it more difficult to accurately compare the simulated and measured results.

This can also be explained in terms of the components in equation (6). Whilst the trimming of SAR images results in $\gamma_{baseline} = 1$ other components such as γ_{RCS} would have played a significant role in reducing the coherence.

So whilst it is possible to achieve good coherence using non-overlapping transmitter trajectories (shown in the simulations) this was not demonstrated in the measured data.

Multistatic collections may provide improved CCD results, however if the component SAR geometries are not carefully chosen then the coherence may decrease. It is possible that the multiple passes (with additional viewing angles) inherent to multistatic images could prove beneficial in change detection, meaning it may not be necessary to form multistatic images for the most interpretable results.

Future work investigating multistatic (and multipass) collections and interferometry may achieve better results with a more tailored change detection algorithm, or potentially using polarimetry and scattering mechanisms to help detect the changes. Such methods might even make the disturbance clear in the measured data. Some of the problems with the measured images may be resolved using a stronger disturbance and improved resolution (bandwidth) measurements in order to achieve similar results to the simulation.

6. Acknowledgements

This paper was produced as part of a PhD project sponsored by the Defence Science and Technology Laboratory (DSTL).

7. References

[1] Bamler, R., Hartl, P.: “Synthetic aperture radar interferometry” Inverse Problems, 1998, 14, (4).
[2] Andre, D.: “Bistatic SAR coherence improvement through spatially variant polarimetry,” in “IMA Conference on Mathematics in Defence” (2015)
[3] Hagelberg, A., Andre, D., Finnis, M.: “Polarimetric bistatic SAR image coherence,” in “14th European Conference on Synthetic Aperture Radar” (VDE, 2022), pp. 80–85
[4] Preiss, M., Stacy, J.: “Coherent Change Detection: Theoretical Description and Experimental Results” (2006)
[5] Andre, D., Morrison, K., Blacknell, D., Muff, D., Nottingham, M., Stevenson, C.: “Very High Resolution Coherent Change Detection,” in “IEEE Radar Conference” (2015)
[6] Andre, D., Blacknell, D., Morrison, K.: “Spatially variant incoherence trimming for improved SAR CCD,” in “SPIE Defense, Security and Sensing” (2013)
[7] Kulu, E.: “Small Launchers-2021 Industry Survey and Market Analysis” (Kepler Communications, 2021)
[8] Bartusch M, Brüns C, Quiroz A, Stettner S: “HRWS: The upcoming German X-Band Spaceborne SAR Mission,” in “EUSAR” (2021)
[9] López-Martínez, C., Pottier, E.: “Basic Principles of SAR Polarimetry,” in “Remote Sensing and Digital Image Processing” (Springer Science and Business Media B.V., 2021), pp. 1–58
[10] Jakowatz, C. v., Wahl, D.E., Eichel, P.H., Ghiglia, D.C., Thompson, P.A.: “Spotlight-mode synthetic aperture radar a signal processing approach” (Kluwer Academic Publishers, 1996)
[11] Zebker, H.A., Member, S., Villasenor, J.: “Decorrelation in Interferometric Radar Echoes” (1992)
[12] André, D., Blacknell, D., Morrison, K.: “Spatially variant incoherence trimming for improved bistatic SAR CCD” (2013)

https://dspace.org/

Non-overlapping trajectory Multistatic SAR Coherent Change Detection

Hagelberg, Alexander; Andre, Daniel; Finnis, Mark V.

2022-10-27
Institution of Engineering and Technology (IET)
https://doi.org/10.1049/icp.2023.1255
Hagelberg A, Andre D, Finnis M. (2022) Non-overlapping trajectory Multistatic SAR Coherent Change Detection. In: IET Radar 2022: International Conference on Radar Systems, 24-27 October 2022, Edinburgh, Scotland

Downloaded from a DSpace repository. https://dspace.org/